Composite Structures 159 (2017) 615–624

Contents lists available at ScienceDirect

Composite Structures

journal homepage: www.elsevier.com/locate/compstruct

Influence of plate length and anchor position on FRP-to-concrete joints anchored with FRP anchors

Huawen Zhang [a], Scott T. Smith [b,*]

[a] Country Garden Group, Foshan, Guangdong Province, China
[b] School of Environment, Science and Engineering, Southern Cross University, Lismore, 2480, NSW, Australia

ARTICLE INFO

Article history:
Received 16 May 2016
Revised 30 August 2016
Accepted 28 September 2016
Available online 28 September 2016

Keywords:
Concrete
FRP
FRP anchors
Joints
Load-slip model
Partial interaction model

ABSTRACT

This paper presents the details of an experimental and analytical study that addresses the influence of fibre-reinforced polymer (FRP) anchors upon the strength and behaviour of FRP-to-concrete bonded interfaces. Single-shear joints are utilised to represent the bonded interface. The primary variables under consideration are (i) the influence of anchor position in relation to the loaded end of the joint, l_{anc}, (ii) the length of plate between the anchor and the unloaded plate end, l_{end}, and (iii) total length of plate, l_{frp}. These variables, which have received limited direct attention to date by the research community, are important parameters for understanding the influence of concrete cracking upon the behaviour of the FRP strengthening systems containing anchorage devices. The results of forty-one anchored joints and two unanchored control joints are presented and it is shown that l_{end} is more influential than l_{anc}. Details of a partial interaction model are also presented and the model is shown to adequately replicate the load, slip and strain distribution responses of a selected test joint.

1. Introduction

Fibre-reinforced polymer (FRP) composites provide a viable strengthening and repair solution when externally bonded onto reinforced concrete (RC) members [1]. The propensity of the FRP plate to debond in a generally brittle manner, at levels of strain considerably lower than the FRP strain capacity, is a severe limitation to the strengthening technology. Novel fabric-reinforced cementitious matrix (FRCM) materials are under investigation in order to improve the bond of the FRP with the substrate [2]. Alternatively, anchorage of the FRP is another approach to enhance the bond capacity. Recent reviews of a variety of anchorage devices incorporated into FRP-strengthened RC structures are provided in Kalfat et al. [3] and Grelle and Sneed [4]. Anchors made from FRP (herein *FRP anchors*) are one effective type of anchorage device which can be applied to RC members of a variety of shapes that have been strengthened with FRP plates. For example, the addition of FRP anchors has been used successfully to enhance the ductility of FRP-strengthened RC slabs and the bonded strain capacity of the FRP plates [5–7]. One key issue that has received no direct research treatment though has been the influence of crack position on the efficiency of FRP-strengthened RC members anchored with FRP anchors. The research presented in this paper addresses this knowledge gap.

Single-shear FRP-to-concrete joints are a convenient means with which to investigate the properties of FRP-to-concrete bonded interfaces [e.g. [8]]. Such joints provide a simple yet reasonably accurate approximation of intermediate crack induced debonding (also known as IC debonding) that can occur in FRP-strengthened RC members [9]. The leading loaded end of the concrete block in the joint test set-up represents a crack in an RC member. The application of FRP anchors to the joint enables the influence of FRP anchors upon the FRP-to-concrete bonded interface to be investigated. Such a test arrangement has been effectively used by the authors of this paper [e.g. [10–12]]. For example, this set-up has the ability to investigate the influence of crack position on FRP-to-concrete bonded interfaces anchored with FRP anchors. In this case, the influence of FRP anchor position in relation to a crack in an RC member can be investigated by locating the anchor at a specified distance from the loaded end of the concrete block in joint shear tests. The joint test setup has also allowed the investigation of other key parameters to date such as the angle of anchor insertion into the concrete member, in addition the influence of the anchor fan.

Fig. 1 is a photograph of a hand-made FRP anchor. The anchor is comprised of two components, namely (i) *anchor dowel*, and (ii) *anchor fan*. The anchor dowel is epoxied into the concrete member

* Corresponding author.
E-mail address: scott.smith@scu.edu.au (S.T. Smith).

http://dx.doi.org/10.1016/j.compstruct.2016.09.086
0263-8223/

Fig. 1. FRP anchor.

and the anchor fan is bonded onto the surface of the FRP plate. The FRP anchor fibres are passed through the FRP plate and when installed, the FRP anchor and FRP plate form a monolithic unit. In this application and from herein, the FRP plate is made in a wet lay-up procedure from carbon fibre sheets. In addition, the FRP anchors are inserted between the yarns during the wet-lay-up application procedure. A large experimental program dealing with the influence of FRP-to-concrete bonded interfaces anchored with FRP anchors shown in Fig. 1 is provided in Zhang [13].

This paper primarily reports an experimental investigation and it is supplemented by a numerical component that provides further insights not gleaned from the tests. The experimental component presents the details and results of 41 FRP-to-concrete joints of which a single anchor was applied to each joint. There were in addition two unanchored control joints. The primary test variables for the anchored joints were (i) position of anchor relative to the loaded bonded plate end (l_{anc}), (ii) length of plate between the FRP anchor and unloaded plate end (l_{end}), and (iii) total plate length (l_{frp}). Joint behaviour and failure modes, load-slip responses, strain efficiency and strain distribution responses, as well as suitable discussions are then presented. The numerical component contains a brief over-view of a partial interaction model. A load-slip model for FRP anchors is also presented. Load, slip and strain distribution responses are generated for one of the test joints and they enable insights to be gained with regards to the influence of the anchor in relation to the total length of plate. A detailed account of the experimental and numerical components of a wider investigation on FRP anchors is provided in Zhang [13].

2. Experimental details

2.1. Details of test specimens

The experimental program consisted of testing 43 joint specimens, with and without anchors, in single shear to failure. Fig. 2 shows the joints details while Fig. 3 shows the test set-up. The concrete blocks were nominally 200 mm wide by 200 mm deep by 400 mm long, and the tested average concrete compressive cube strength was 55 MPa. The same type of carbon fibre sheet was used to make the FRP anchors and the FRP plate. The fibre sheet was nominally 0.131 mm thick per layer and FRP plates of 50 mm width were made from three layers of carbon fibre sheet in a wet lay-up manner. An unbonded zone of 40 mm length which was created by inserting a thin sheet of plastic between the concrete and epoxy, was maintained for all the specimens at the loaded edge of the concrete blocks. The tests reported in this paper, of which the main test parameters are summarised in Table 1 and the symbols are defined in Fig. 2, are divided into four series. The main parameters under investigation are (i) position of anchor relative to the loaded bonded plate end (l_{anc}), (ii) length of plate between the anchor and unloaded plate end (l_{end}), and (iii) total plate length (l_{frp}). Each series is described in detail as follows in the context of Table 1 and Fig. 2.

2.1.1. Control (CN) series

Control tests were performed on two unanchored FRP-to-concrete joints of 250 mm bonded plate length, l_{frp}. According to Chen and Teng [14], the effective bond length L_{eff} ($L_{eff} = \sqrt{E_{frp} t_{frp} / \sqrt{0.8 f_{cu}}}$) as calculated for the geometric and material properties of the control joints, was 116 mm (herein 120 mm). For this bond length equation, E_{frp} and t_{frp} are the elastic modulus (MPa) and thickness (mm) of FRP, respectively, and f_{cu} is the cube compressive strength of concrete (MPa). The 250 mm length was deliberately selected in this study to be much longer than L_{eff} for several reasons, namely (i) serve as a default length of plate, (ii) more readily observe debonding crack propagation, (ii) sufficient length for a variety of anchor positions to be explored, and (iii) more readily extract the contribution of the anchor.

2.1.2. Series A (variable l_{anc} and l_{end}, constant l_{frp})

The bonded plate length was maintained at 250 mm while four different l_{anc} values were investigated, namely 75 mm, 125 mm, 175 mm and 225 mm. The corresponding l_{end} values 175 mm, 125 mm, 75 mm and 25 mm.

2.1.3. Series B (variable l_{anc} and l_{frp}, constant l_{end})

Previous tests on FRP-to-concrete joints anchored with FRP anchors [e.g. [12]] have shown the initiation of plate debonding to occur at approximately the same load as debonding initiation in unanchored control joints. The load capacity of the anchored joint may therefore be independent of l_{anc}. This series tests the hypothesis that the load capacity of the anchored joint is dependent on l_{end} rather than on l_{anc}. Two different values of l_{end} were investigated, namely, 25 mm and 125 mm. These lengths were less than and greater than Chen and Teng's [14] effective bond length, respectively. For each value of l_{end}, four different values of l_{anc} were investigated, namely, 75 mm, 125 mm, 175 mm and 225 mm. As a consequence of these variables, l_{frp} varied according to the geometry of the plate.

2.1.4. Series C (variable l_{end} and l_{frp}, constant l_{anc})

The influence of l_{frp} was investigated in this series. The anchor was positioned at a constant location (i.e. l_{anc} = 75 mm) while l_{frp} was varied from 100 mm to 350 mm in 25 mm intervals. As a result of variable l_{frp}, l_{end} was also varied.

Two tests were initially conducted for each of the test permutations shown in Table 1. A third and even a fourth test of the same configuration was undertaken if the variation of the results from the first two tests was excessive (i.e. peak load difference greater than 10%). In addition, selected test permutations were used multiple times as identified in Table 1 due to repetition of parameters. As a result, there are 54 specimens identified in Table 1 although there were 43 actual joint tests. Note that the specimen identification used in Table 1 is different to that used by Zhang [13].

2.2. Construction of FRP anchors and FRP-to-concrete joints

A detailed account of anchor manufacture and assembly is contained in Zhang [13]. A brief overview is provided herein.

A rectangular portion of uni-directional carbon fibre sheet of 150 mm length (in direction of fibres) and 200 mm width was initially cut (note that the 150 mm long rolled fibres were trimmed to the required length of 90 mm after insertion of the anchor into the concrete). Epoxy was applied to an end portion extending 25 mm

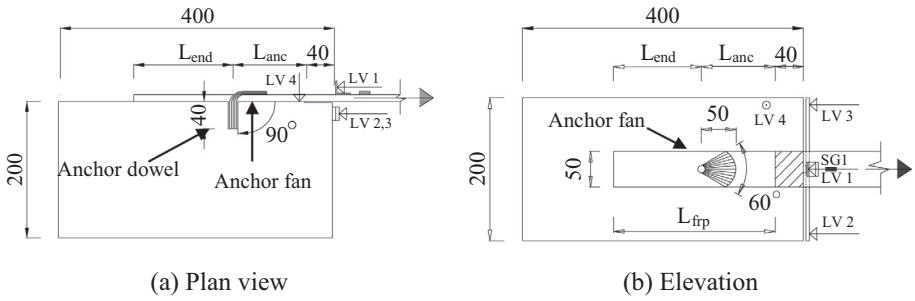

Fig. 2. Specimen geometry, labelling and instrumentation.

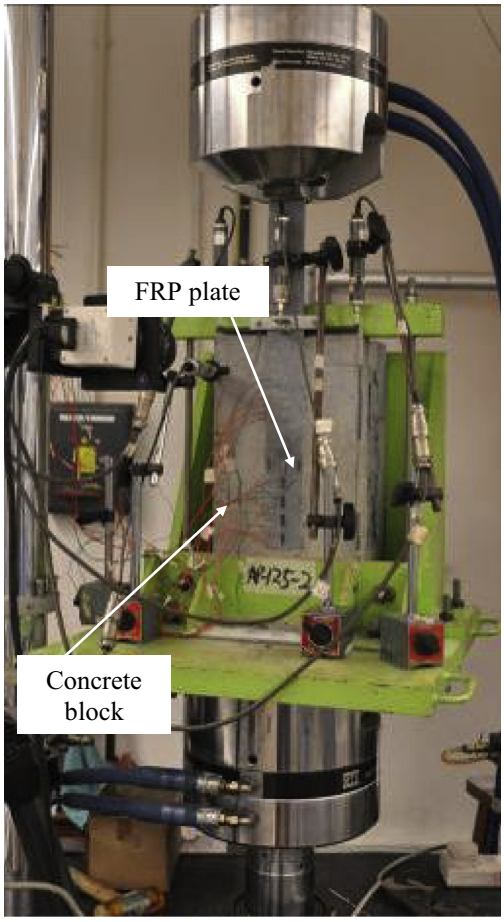

Fig. 3. Test set-up.

across the whole width of the sheet for the formation of the anchor dowel component. This type of anchor is therefore referred to as an impregnated anchor. The fibre sheet was then rolled from one longitudinal side to the other. In order to form the anchor dowel shape, the rolled impregnated end was inserted into epoxy filled holes of 12 mm diameter which were pre-drilled into polystyrene blocks. The rolled fibres were then removed after one day to produce FRP anchors as shown in Fig. 1.

Prior to installation of the anchor, a 14 mm diameter hole was drilled into the concrete and then the area of concrete to be strengthened with an FRP plate was prepared by removing the top few millimeters of concrete with a pneumatic needle scaler. The prepared concrete surface and drilled anchor hole were then cleaned by spraying with compressed air. The hole was next injected with epoxy, and then the anchor dowel inserted into the hole. The plate was then formed onto the prepared concrete using the wet lay-up technique. The advantage of using fibre sheets, as opposed to pultruded plates, was that the dry fibres in each sheet layer could be locally parted in order to be slipped over the anchor during installation. No drilling of holes in the plate was therefore necessary. Finally, after the plate was formed, the anchor fan fibres were then splayed and epoxied onto the surface of the plate by the same epoxy used to form the plate. Each specimen was then allowed seven days to cure prior to testing within an air-conditioned environment.

2.3. Test set-up, instrumentation and loading

The single-shear test set-up is shown in Fig. 3. This arrangement was selected because it was simple and repeatable, and the specimens were relatively easily handled and assembled. The concrete block was completely restrained by a steel holding frame which was mounted inside a MTS 250kN 810 universal testing machine. In all cases, 260 mm of plate extended out from the loaded end of the concrete block of which 60 mm was gripped by the jaws of the universal testing machine under a pressure of 10 MPa. Load was applied in a ram displacement control manner at a constant rate of 0.3 mm/min. An initial load of 5 kN was applied to all test specimens in order to bed each specimen and test instrumentation. The initial load was then removed in order to commence the actual test from zero load. During this unloading process, no noticeable repositioning of the test specimen was observed. Load was then applied monotonically until specimen failure.

Fig. 2 shows the generic layout of the LVDTs (denoted as LV) in addition to the location of an electric resistance strain gauge (denoted as SG1) of 10 mm gauge length. This strain gauge was located 100 mm from the loaded bonded end of the plate. The four LVDTs were used to monitor plate and concrete block movements. LV1 measured the in-plane displacement of the FRP plate 45 mm from the loaded bonded end of the joint. LV2 and LV3 were mounted onto a metallic arm spanning the width of the concrete block which was connected to the centre of the block behind the FRP plate. The relative movement between the loaded bonded end of the FRP plate to the concrete block was obtained by subtracting the average value of LV2 and LV3, and the extension of the FRP plate between the loaded bonded end to the location of LV1 (i.e. 45 mm plate length). Elastic extension of the plate in the unbonded region was considered although concrete deformation between LV2 and LV3 to the bonded end of the plate was neglected owing to the much stiffer concrete in relation to the FRP plate. Such relative movement is herein referred to as plate-end slip or more

Table 1
Details of test specimens.

Series and Specimen ID[1]		Plate and Anchor Details			Additional Details	
		l_{anc} (mm)	l_{end} (mm)	l_{frp} (mm)	Identical Specimens[2]	Fibre Roll[3]
Control	CN-1 ~ 2	–	–	250		R2
Series A	A1-1 ~ 2	75	175	250	*	R2
	A2-1 ~ 2	125	125	250	**	R1
	A3-1 ~ 4	175	75	250		R1
	A4-1 ~ 2	225	25	250	***	R1
Series B	B1-1 ~ 2	75	25	100	#	R1
	B2-1 ~ 2	125	25	150		R2
	B3-1 ~ 2	175	25	200		R2
	B4-1 ~ 2	225	25	250	***	R1
	B5-1 ~ 3	75	125	200	##	R1 = 1 ~ 2: R2 = 3
	B6-1 ~ 2	125	125	250	**	R1
	B7-1 ~ 2	175	125	300		R2
	B8-1 ~ 2	225	125	350		R2
Series C	C1-1 ~ 2	75	25	100	#	R1
	C2-1 ~ 2	75	50	125		R2
	C3-1 ~ 2	75	75	150		R1
	C4-1 ~ 2	75	100	175		R2
	C5-1 ~ 3	75	125	200	##	R1 = 1 ~ 2: R2 = 3
	C6-1 ~ 2	75	150	225		R1
	C7-1 ~ 2	75	175	250	*	R2
	C8-1 ~ 2	75	200	275		R2
	C9-1 ~ 2	75	225	300		R2
	C10-1 ~ 3	75	250	325		R2
	C11-1 ~ 3	75	275	350		R2

[1] 1 ~ 2 = specimens 1 and 2.
[2] Identical specimens are indicated via matching symbols (e.g. ***means that specimens A4-1 ~ 2 and B4-1 ~ 2 are identical).
[3] R1 = carbon fibre sheet roll 1, R2 = carbon fibre sheet roll 2.

simply *slip*. LVDT 4 monitored the out-of-plane movement of the concrete block. The resulting out-of-plane movements of the blocks were mostly less than 1 mm and hence deemed to be sufficiently small. Such movement has been proved to have little influence on test results [8].

While not shown on Fig. 2, additional strain gauges of 10 mm gauge length were bonded along the entire length of bonded plates for several test specimens. A strain gauge was bonded 10 mm from the loaded bonded plate end with the remaining gauges bonded at 25 mm intervals. Should an intended strain gauge position have rested within the anchor fan region then the gauge was omitted.

2.4. Material properties

Two rolls of the same type of carbon fibre sheet were used. They are identified as R1 (roll 1) and R2 (roll 2) in Table 1. The material properties of both rolls of fibre sheet were determined in accordance with ACI 440.3R-04 [15] using 30 mm wide flat coupon tension specimens formed in a wet lay-up manner from two layers of carbon fibre sheet. The properties of the first and second roll, averaged from five coupons per roll, were; ultimate strain = 15040 με and 13400 με (standard deviation, sd. = 930 με and 808 με), tensile strength = 3065 MPa and 2978 MPa (sd. = 162 MPa and 201 MPa), and modulus of elasticity = 224 GPa and 227 GPa (sd. = 7 GPa and 6 GPa), respectively. The joint tests presented in the results section of the paper achieved at most 58% of the strain capacity of the plates. As the test plates did not rupture, elastic modulus is identified as the most important material property with regards to analysis and modelling. As a result, the material properties of the plates arising from the two rolls of carbon fibre sheet can be considered near identical upon consideration of elastic modulus.

Seven dog-bone specimens with a minimum cross-section of 4.6 mm by 9.8 mm were tested in accordance with BS EN ISO 527:1996 [16] in order to determine the material properties of the adhesive. The stress-strain responses arising from the coupons were found to be largely linear-elastic. The specimens produced an average ultimate strain = 6716 με (s.d. = 428 με), tensile strength = 28 MPa (s.d. = 1.5 MPa), and modulus of elasticity = 4.3 GPa (s.d. = 0.11 GPa).

All the concrete blocks were poured in one batch from commercially sourced concrete of 20 mm maximum aggregate size. The concrete material properties were tested in accordance with the BS 1881 [17–20] suite of standards during the same time as the joint tests and when the concrete was mature (more than half a year). The results, averaged from three specimens, produced a compressive cube strength = 55.1 MPa, modulus of elasticity = 30.2 GPa, splitting strength = 3.6 MPa, and modulus of rupture of 6.2 MPa.

3. Experimental results

This section reports experimental results of (i) selected load versus slip responses (Fig. 4), (ii) behaviour and failure modes (Fig. 5), (iii) strength enhancement of anchored joints relative to control joints (Fig. 6), and (iv) strain distributions (Fig. 7). A summary of averaged key values of load and slip, as well as plate strain efficiency and failure modes is provided in Table 2. Discussions are provided throughout where necessary and relevant.

3.1. Behaviour and failure modes, and load-slip responses

3.1.1. Control joints

All unanchored control joints failed by debonding in the concrete at the FRP-to-concrete interface. This failure mode is expected and it also confirms the quality of the application of the FRP material. Prior to debonding, the relationship between load and slip was relatively uniform. Debonding initiated at the loaded end of the joint at load P_{db} and slip s_{db}, and propagated to a length approximately equal to the effective bond length of about 120 mm. As the debonding cracks then propagated towards the unloaded plate end, the load plateaued. The load reached a maximum during the debonding process and the peak load is defined as $P_{max,1}$. In

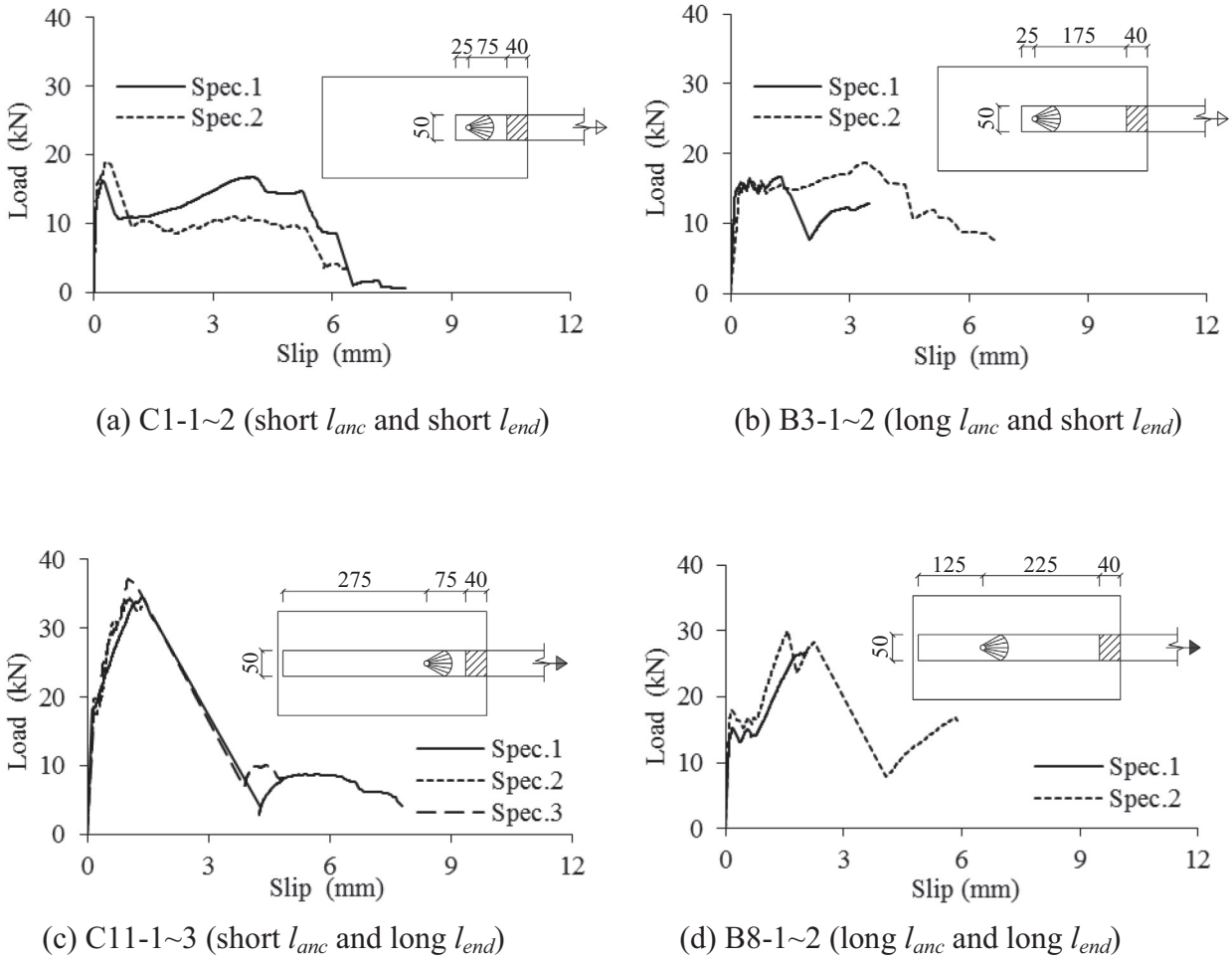

Fig. 4. Selected load-slip responses.

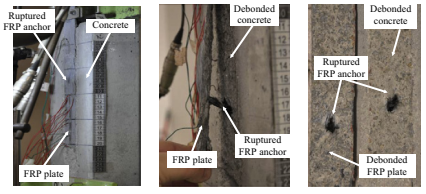

Fig. 5. Typical anchored joint failure (Specimen A3-1).

addition, the maximum slip that the joint could resist is defined as $s_{max,1}$. This behaviour has been extensively documented in the open literature [e.g. 8]. Average key values of load and slip, as well as failure mode, are provided in Table 2 for specimens CN-1 and CN-2.

3.1.2. Anchored joints

The load-slip responses of all anchored joints can be divided into three portions as idealised in Fig. 8 from test results [12], namely (1) linear ascending portion (pre-debonding), (2) debonding propagation portion, and (3) post-debonding portion. The coordinates (P_{db}, s_{db}) and ($P_{max,1}$, $s_{max,1}$) are the load and slip at the boundaries of portions 1 and 2, and 2 and 3, respectively. In addition, $P_{max,2}$ and $s_{max,2}$ are the maximum load and corresponding slip within the post-peak reserve of strength region that exists within the third portion. A summary of these key load and slip results, in addition to failure modes, is contained in Table 2. Four different trends in the load-slip responses were observed and an example of each trend is provided in Fig. 4. Descriptions of the trends are provided as follows in relation to each of the three portions identified at the beginning of this paragraph.

Portion 1: The first portion behaved in a similar manner to the control joints prior to debonding initiation. Table 2 shows that the load P_{db} for the anchored joints was similar to the control joints. The corresponding slip at debonding, s_{db}, was generally less for the anchored joints. This was on account of enhanced FRP plate stiffness over a portion of its length arising from the anchor fan fibres, albeit a small portion.

Portion 2: This portion commenced with the initiation of the debonding cracks at the loaded end of the joint. The debonding cracks then propagated to a length approximately equal to the effective bond length of about 120 mm. The load-slip responses, however, then exhibited four different behaviours and these responses are dependent on the anchor position and the plate length. These behaviours are therefore related qualitatively to dimensions l_{anc} and l_{end}, namely (i) short l_{anc} and short l_{end} (e.g. Fig. 4a), (ii) long l_{anc} and short l_{end} (e.g. Fig. 4b), (iii) short l_{anc} and long l_{end} (e.g. Fig. 4c), and (iv) long l_{anc} and long l_{end} (Fig. 4d). *Short* and *long* are defined as less than and greater than Chen and Teng's [13] effective bond length, l_{eff}, respectively

(i) *short l_{anc} and short l_{end}* (e.g. Specimen C1): As the anchor was positioned within the effective bond length region (i.e. 75 mm < 120 mm), debonding crack propagation was halted

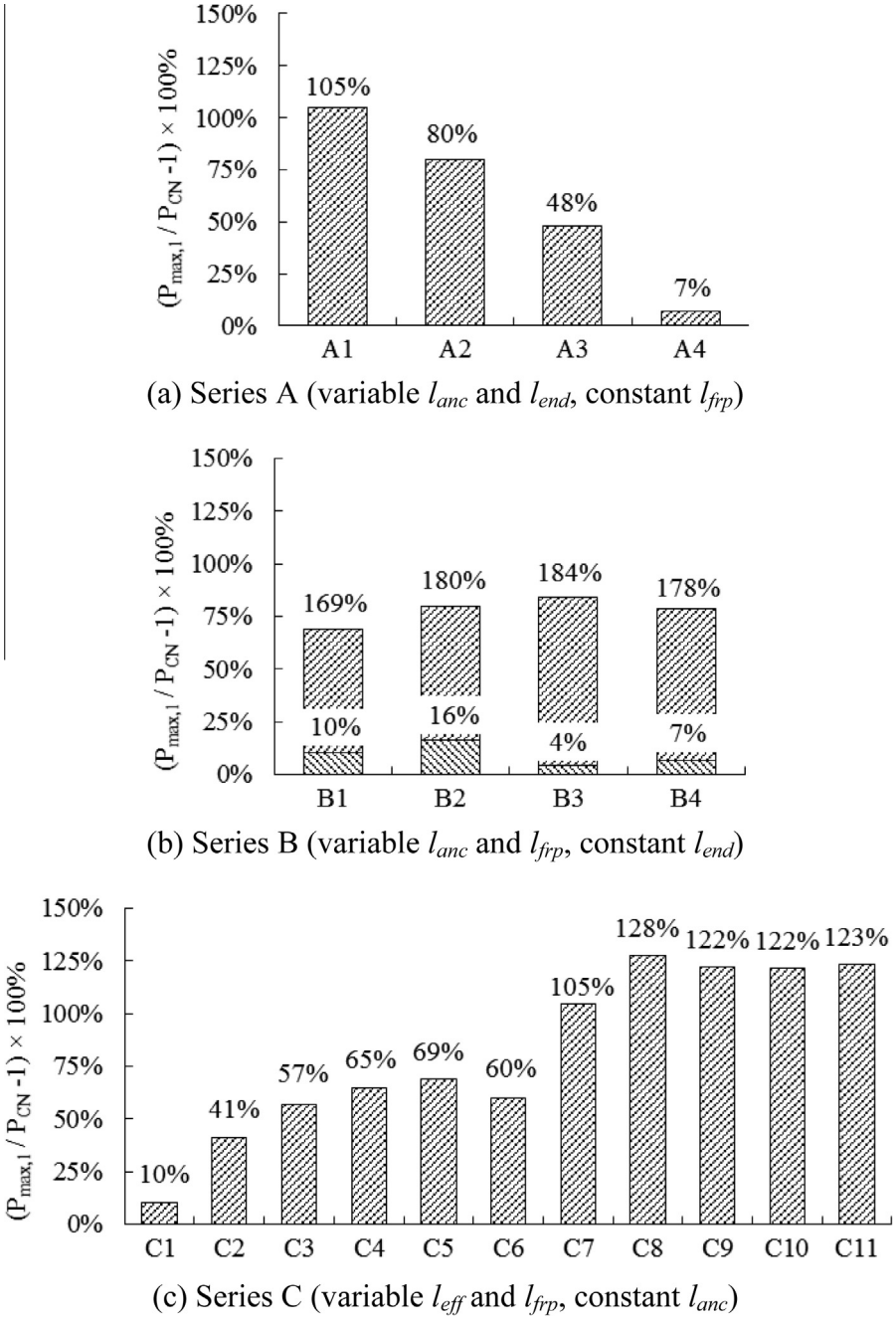

Fig. 6. Anchored joint strength enhancements over control specimens.

by the anchor before it could propagate to length l_{eff}. The anchor did contribute though to the enhancement of peak load, $P_{max,1}$, of about 10% above the peak load of control specimens as shown in Table 2. As debonding propagated past the anchor, there was little increase in load owing to the short length l_{end}. The reduced slip at P_{db}, compared to the control joints, is due to added stiffness provided to the joint by the anchor.

(ii) *long l_{anc} and short l_{end}* (e.g. Specimen B3): The debonding crack initiated at the loaded bonded end. The load then plateaued as evident in Fig. 4b and the slip increased as the debonding crack propagated to the anchor position. During this plateau stage, the joint was acting essentially as a control joint and the anchor had slight influence. As observed in point (i), the small l_{end} (25 mm) meant that the contribution of the anchor was limited as the debonding crack propagated past the anchor towards the plate end. This is reflected by a small increase of 4% in $P_{max,1}$ above the strength of the control specimens. However, a greater l_{anc} produced more ductile behaviour compared to a shorter l_{anc}.

(iii) *short l_{anc} and long l_{end}* (e.g. Specimen C11): The debonding crack propagation was halted by the anchor once the debonding crack initiated from the loaded bonded end. As the debonding cracks propagated along the long l_{end} of 275 mm, the FRP anchor was engaged and the load increased with slip as evident in Fig. 4c. The average peak load, $P_{max,1}$, of the anchored joints compared to the control joints was 123% in excess as per Table 2.

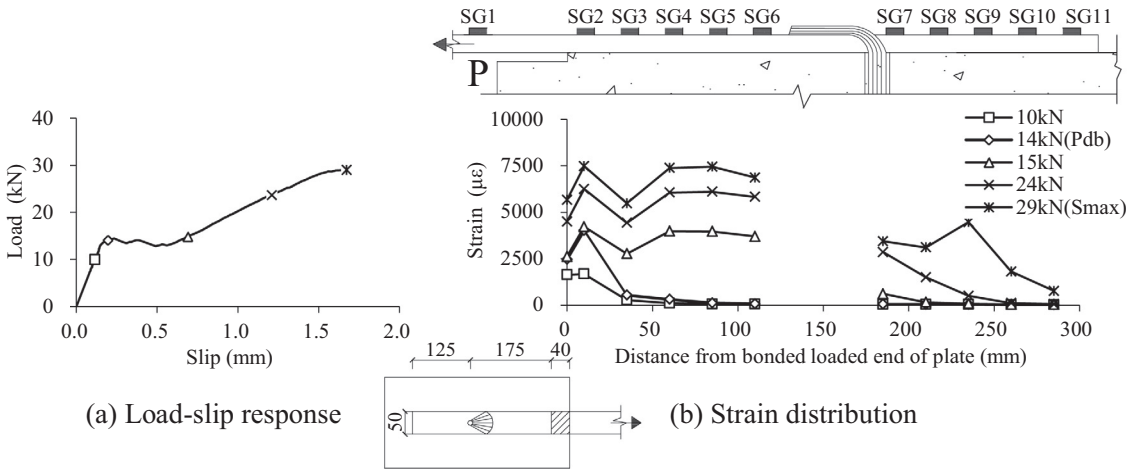

Fig. 7. Selected strain distributions (Specimen B7-2).

Table 2
Selected average test results.

Specimen and Series Identification		P_{db} [a] (kN)	s_{db} [a] (mm)	$P_{max,1}$ [a] (kN)	$s_{max,1}$ [a] (mm)	$P_{max,2}$ [a] (kN)	$s_{max,2}$ [a] (mm)	Strain Efficiency[b]	Failure Mode[c]
Control series	CN	15.46	0.25	15.88	0.91	–[d]	–	0.26	DB
Series A	A1	15.88	0.09	32.51	0.86	15.37	5.43	0.46	2A
	A2	14.74	0.11	28.53	0.98	11.68	3.53	0.40	2A
	A3	15.38	0.14	23.49	1.12	12.43	4.99	0.38	2A
	A4	15.15	0.15	16.97	0.88	12.08	4.16	0.32	2A
Series B	B1	14.48	0.08	17.54	0.27	13.85	3.66	0.23	2A
	B2	14.44	0.18	18.44	0.61	17.43	0.94	0.29	2A
	B3	15.53	0.21	16.57	0.87	15.78	3.45	0.31	2A
	B4	15.15	0.15	16.97	0.88	12.08	4.16	0.32	2A
	B5	15.92	0.12	26.83	0.75	15.16	3.98	0.43	2A
	B6	14.74	0.11	28.53	0.98	11.68	3.53	0.40	2A
	B7	14.08	0.27	29.24	1.58	11.41	3.72	0.44	2A&1A
	B8	16.61	0.17	28.34	1.82	16.71	5.83	0.56	1A&2A
Series C	C1	14.48	0.08	17.54	0.27	13.85	3.66	0.30	2A
	C2	15.35	0.32	22.40	0.61	17.41	3.21	0.38	2A
	C3	15.43	0.08	24.87	0.54	12.57	4.80	0.42	2A
	C4	13.60	0.08	26.17	0.65	13.82	2.74	0.48	2A
	C5	15.92	0.12	26.83	0.75	15.16	3.98	0.42	2A
	C6	17.37	0.18	25.43	0.81	10.93	4.66	0.33	2A
	C7	15.88	0.09	32.51	0.86	15.37	5.43	0.46	2A
	C8	20.28	0.18	36.15	1.03	11.76	4.12	0.58	1A&2A
	C9	17.58	0.14	35.31	1.22	12.80	3.53	0.53	2A&1A
	C10	15.41	0.13	35.20	1.06	9.09	4.07	0.56	2A
	C11	18.55	0.17	35.44	1.11	9.39	5.05	0.54	2A,1A&2A

[a] P_{db} and s_{db}: load and slip at debonding initiation; $P_{max,1}$, $s_{max,1}$: maximum load and corresponding slip at full plate debonding; $P_{max,2}$, $s_{max,2}$: maximum post-peak load and corresponding slip.
[b] Average of maximum strain measurements (SG1) divided by ultimate strain of FRP plate.
[c] DB = plate debonding; Mode 2A = plate debonding followed by anchor rupture; Mode 1A: Simultaneous plate debonding and anchor shear failure.
[d] not applicable.

(iv) *long l_{anc} and long l_{end}* (e.g. Specimen B8): As observed in case (ii), the load plateau is also evident in Fig. 4d as the debonding cracks propagated within the long l_{anc} region. As the debonding cracks propagated within the l_{end} region, the load then increased. The average increase in $P_{max,1}$ for the anchored joint over the control joints was 78%.

Portion 3: The third portion of the load-slip responses occurred following complete plate debonding. As the debonding cracks reached the plate end and hence the plate fully detatched from the concrete block, load was released as evident from the large load drops (and slip increases) shown in each curve presented in Fig. 4. In most cases, the FRP anchor was left intact due to its ability to deform in its bend region. A post-peak reserve of strength and enhanced slip capacity was achieved on account of the frictional resistance of the fully debonding plate and resistant force provided by the anchor. The load-slip responses terminated as the anchors ruptured in the bend region (i.e. mode 2A failure). In a limited number of cases which are identified in Table 2 (i.e. mode 1A failure), anchors ruptured simultaneously as the plate fully debonded. For this failure mode, no third region in the load-slip response was observed for this failure mode.

The failure modes of the anchored joints can therefore be summarised as follows using a convention initially reported in Kim [21]

- *Mode 1A: Simultaneous plate debonding and anchor rupture*
- *Mode 2A: Plate debonding followed by anchor rupture*

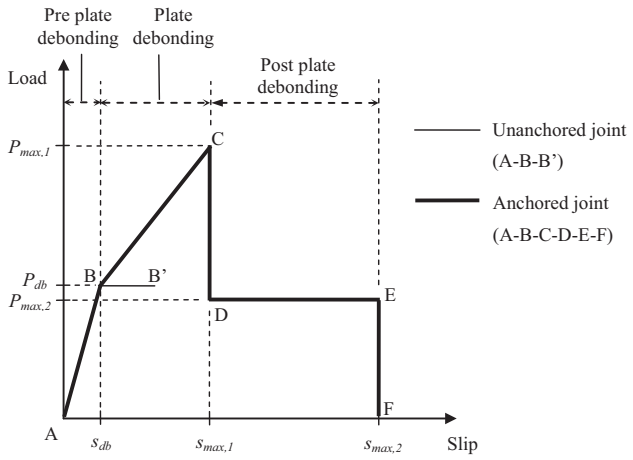

Fig. 8. Generic load-slip responses of unanchored and anchored joints.

Fig. 5 shows a typical Mode 2A failure although a Mode 1A failure will look the same. The ruptured FRP anchor fibres are evident as well as the debonding in the concrete at the FRP-to-concrete interface. The concrete attached to the FRP plate is at most a few millimetres in thickness. Joints with higher $P_{max,1}$ tended to fail in a Mode 1A manner. This failure mode is undesirable as it will not allow a post-peak reserve of strength and associated slip capacity to be achieved. Anchor failure was exacerbated by the large release of energy at plate debonding. Mode 2A is more desirable and more likely to occur. To minimise the likelihood of Mode 1A failure in joints subjected to large loads, anchors containing more fibre can be considered.

3.2. Strength enhancement

A summary of the average anchored joint strengths, $P_{max,1}$, for each test permutation, in relation to the average control joints peak load (P_{CN}) are provided in this section. The results are presented based on the series groupings provided in Table 1.

3.2.1. Series A (variable l_{anc} and l_{end}, constant l_{frp})

The reader is referred to the results presented in Fig. 6a for the influence of l_{anc} and l_{end} with constant plate length. The capacities of the anchored joints more than doubled for optimal anchor positioning but increased ever slightly (i.e. 7%) for non-optimal anchor positioning. In summary, the anchored joint strengths are shown to decrease for increasing l_{anc} and decreasing l_{end}. It is not possible though to properly grasp the relationship between l_{anc} and l_{end} upon $P_{max,1}$ based on this series of tests. Recourse is therefore made to the Series B and C tests reported in this paper.

3.2.2. Series B (variable l_{frp} and l_{anc}, constant l_{end})

Fig. 6b presents a summary of the series B peak load results of which the percentages indicated at the top and the bottom of the bars correspond to l_{end} = 125 and 25 mm, respectively. It is evident that the joint strengths increased as l_{end} increased. As l_{anc} was increased though within each sub-set of constant l_{end}, the joint strengths remained reasonably constant with no evident trend within the variation. The dimension l_{end} would therefore appear to be more influential than l_{anc}.

3.2.3. Series C (variable l_{end} and l_{frp}, constant l_{anc})

The results presented in Fig. 7c show that joint strength increases with increasing l_{end}. The joint strengths, however, plateaus as l_{end} exceeds 200 mm. This represents an effective bond length for the entire anchored joint. It is hypothesised that the effective bond length is dependent upon the material and geometric properties of the joint. Further investigation of effective bond length in anchored joints is left for future studies.

3.3. Strain efficiency and strain distribution

The second last column of Table 2 lists the average FRP plate strain efficiency of each test permutation. The efficiency is calculated by dividing the average peak strain (i.e. SG1 value for each test joint) by the tested ultimate strain capacity of the FRP plate. The average strain efficiency for the control joints was 26%. The highest average strain efficiency for the anchored joints was 58%. As the focus of this study was on understanding the relationship between l_{anc}, l_{end} and l_{frp}, future studies may focus on maximising plate strain efficiency.

Fig. 7 shows the load-slip and strain distribution responses for a typical joint of which l_{anc} and l_{end} were long (i.e. l_{anc} = 175 mm, l_{end} = 125 mm for joint B7-2). Long lengths have been used so a sufficient number of strain gauge results over each region can be analysed in order to draw meaningful conclusions. The distinct stages in the load-slip response are therefore evident, namely (i) pre-debonding uniform relationship between load and slip, (ii) debonding propagation load plateau (i.e. due to propagation of debonding cracks from lengths l_{eff} to l_{anc}), and (iii) debonding propagation load increase (i.e. due to propagation of debonding cracks from lengths l_{anc} to l_{frp}). There is no post-peak reserve of strength for this joint on account of Mode 1A failure. Nonetheless, post-peak responses are not relevant for strain anyway. Strain distributions at key levels of load (and slip) are provided in Fig. 7b and the levels of load are related to key stages in the load-slip response. The propagation of debonding along the length of the plate between the loaded end of the joint and the anchor is evident for the distributions corresponding to the load level of 14kN and 15kN. For the latter, the strain distribution is reasonably constant which corresponds to debonding. This constant distribution increases in magnitude as the load is increased. The increase of strain in gauges SG7-SG10 is evident for the last three load steps. The maximum strain in the l_{end} region when the plate fully debonded from concrete is approximately the same as the strain at the loaded bonded end when the debonding initiated. Consistently low levels of strain for gauge SG11 means the free end of the plate is not greatly strained throughout the entire process. There are understandably no strain results within the anchor fan region due to the fan fibres thickening the plate. Overall inspection of Fig. 7b shows that the most heavily stressed portion of plate exists between the loaded end and the anchor. The anchor fan fibres that locally thicken the plate act in a beneficial manner.

4. Modelling

This section reports selected results of a partial interaction model applied to FRP-to-concrete joints anchored with FRP anchors that aim to supplement the tests presented in this paper. The model is used to investigate (i) the ability to simulate the load-slip response of FRP-to-concrete joints anchored with FRP anchors, (ii) investigate the distribution of strain for short l_{anc} (i.e. such a short length was not adequately monitored by a sufficient number of strain gauges in the experimental portion of the paper), and (iii) the anchorage provided by l_{end}.

The model was originally developed to analyse steel reinforcing bars embedded in concrete by Haskett et al. [22]. It has also been modified to consider FRP-to-concrete bonded interfaces [23]. A load-slip (P-s) model for FRP anchors reported in Zhang and Smith [24] is added to Zhang et al.'s [23] version of the model and selected results are reported herein. This model can be used to gen-

erate load-slip and strain distribution responses and a typical test joint is analysed herein.

The modelling approach involves discretising the joint into a series of elements oriented perpendicular to the longitudinal axis of the plate as shown in Fig. 9a. Equilibrium and compatibility conditions, as well as boundary conditions, are enforced during an iterative solution process of which the model is activated by displacing the slip at the loaded end of the bonded FRP plate. Once a level of load applied to the plate is assumed, the slip, strain and stress in each consecutive element is calculated in succession and then the boundary conditions at the free end of the plate are assessed. The load is incremented and the analysis repeated until the boundary conditions are satisfied. The slip is then incremented and the analysis is repeated until the limit state of complete plate debonding has been reached. A detailed description of the model can be found in Zhang [13].

The sole element at the anchor location utilises the constitutive model of the anchor in the same direction of the loading. The connection between the FRP and concrete for the remaining bonded but unanchored elements is defined by the bond stress-slip response of the FRP-to-concrete bond. Zhang and Smith's [24] constitutive FRP anchor model is shown in Fig. 9b. The key parameters are P_1 = 19.60 kN, s_1 = 0.53 mm and s_2 = 3.82 mm. The slope of the ascending portion is 36.98 kN/mm. These parameters have been obtained from tests as well as analysis, and full descriptions of their derivation are provided in Zhang [13] and Zhang and Smith [24]. A bi-linear bond stress-slip model is proposed as shown in Fig. 9c and it has been calibrated from the control joint CN-1. Associated values are τ_{max} = 5.99 MPa, s_0 = 0.07 mm and s_{max} = 0.20 mm. The anchor model and the bond-slip model are actually of critical importance for the analysis of bonded interfaces containing anchors and they can be used in other numerical modelling techniques such as finite element analysis.

The partial interaction model is applied to joint C10 for the pre-debonding and debonding stages of response. For this particular joint the total plate length is 325 mm of which l_{anc} = 75 mm (i.e. short length) and l_{end} = 250 mm. The model captures the load-slip response well as shown in Fig. 10a although it produces a slightly less stiff response than the three test joints. This may be due to the anchor fan fibres not being included in the model although the fan fibres are localised to the anchor location. Fig. 10b shows the predicted strain distribution and it is consistent with test observations at the selected slip levels. The constant level of strain along portions of the plate length at higher levels of slip indicates debonding and the vertical drop in strain occurs at the anchor location. In addition, higher levels of strain are found in the l_{anc} region as opposed to l_{end} end region. This illustrates the important of the anchor location is relation to the loaded end of the joint, in addition to anchorage provided by the plate between the anchor and the plate end. The partial interaction model is a powerful tool. It enables parametric studies to be undertaken on FRP-to-concrete joints anchored with FRP anchors of variable material and geometric properties. Such studies, which form necessary future work, may enable the development of debonding strength models and generic *P-s* FRP anchor constitutive models.

5. Conclusions

This paper has reported the details and results of an experimental and analytical program which has considered the influence of anchor position and plate length on FRP-to-concrete joints anchored with FRP anchors. More specifically, the parameters investigated were anchor position relative to the bonded loaded joint end (l_{anc}), length of plate from anchor position to unloaded plate end (l_{end}), and total plate length (l_{frp}). The 41 anchored joint tests and arising analysis have yielded the following results that

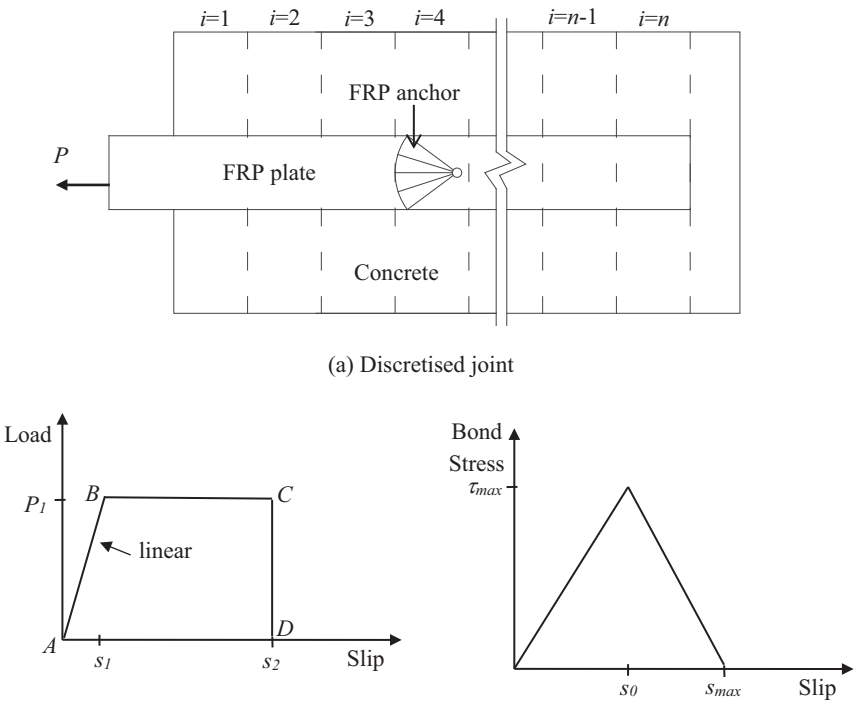

(a) Discretised joint

(b) Load-slip model for FRP anchors

(c) Bond stress-slip model for FRP-to-concrete interfaces

Fig. 9. Partial interaction model details.

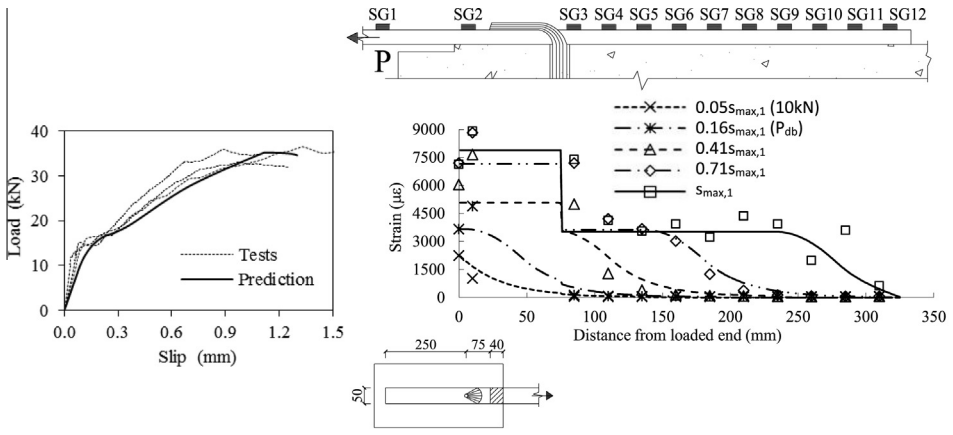

(a) Load-slip responses (b) Strain distribution (lines and symbols correspond to prediction and test, respectively)

Fig. 10. Comparison between tests results and model predictions (Specimen C10).

are valid within the range of the geometrical and material properties considered in the study.

- Three distinct load-slip portions, namely, pre-debonding, debonding propagation, and post-debonding reserve of strength.
- Four distinct trends corresponding to the debonding propagation portion of the load-slip response. In essence, for longer l_{anc} there was a load plateau generated as the debonding cracks propagated from the loaded bonded end to l_{anc}. This plateau is important for enhancing the ductility (and deformation) of the joint. For sufficient lengths of l_{end}, joint strength was increased and the FRP anchor was effectively engaged.
- l_{end} was much more influential than l_{anc} on the ultimate strength of joint. For instance, for constant l_{anc}, the influence of l_{eff} was considerable.
- Existence on an effective bond length for anchored joints which is influenced by l_{end}.
- Plate strain utilisation was increased from 26% (for unanchored joints) to 58% (for anchored joints).

The ability of a partial interaction model to produce load-slip and strain distribution results that replicate the experimental results well was demonstrated. The partial interaction model may be used in future studies to conduct parametric studies in order to understand the influence of a range of material and geometric properties on FRP-to-concrete joints that are anchored with FRP anchors. In addition, the development of guidance for the design of FRP-strengthened structures anchored with FRP anchors is an urgency. The results and observations contained in this paper can be added to the ever increasing pool of anchor information available in the open literature.

Acknowledgements

The resources provided by Southern Cross University and The University of Hong Kong are gratefully acknowledged.

References

[1] Hollaway LC, Teng JG. Strengthening and rehabilitation of civil infrastructures using fibre-reinforced polymer (FRP) composites. Cambridge, UK: Woodhead Publishing Limited; 2008.
[2] ACI 549.4R-13. Guide to design and construction of externally bonded Fabric-Reinforced Cementitious Matrix (FRCM) Systems for repair and strengthening concrete and masonry structures. Farmington Hills, MI, USA: American Concrete Institute; 2013.
[3] Kalfat R, Al-Mahaidi R, Smith ST. Anchorage devices used to improve the performance of concrete structures retrofitted with FRP composites: a-state-of-the-art review. J Compos Constr ASCE 2013;17(1):14–33.
[4] Grelle SV, Sneed LH. Review of anchorage systems for externally-bonded FRP laminates. Int J Concr Struct Mater 2013;7(1):17–33.
[5] Orton SL, Jirsa JO, Bayrak O. Design considerations of carbon fiber anchors. J Compos Constr ASCE 2008;12(6):608–16.
[6] Smith ST, Hu SH, Kim SJ, Seracino R. FRP-strengthened RC slabs anchored with FRP anchors. Eng Struct 2011;33(4):1075–87.
[7] Smith ST, Zhang HW, Wang ZY. Influence of FRP anchors on the strength and ductility of FRP-strengthened RC slabs. Constr Build Mater 2013;49:998–1012. Special Section on Ductility of Civil Engineering Structures Incorporating FRPs.
[8] Yao J, Teng JG, Chen JF. Experimental study on FRP-to-concrete bonded joints. Compos B Eng 2005;36(2):99–113.
[9] Teng JG, Smith ST, Yao J, Chen JF. Intermediate crack induced debonding in RC beams and slabs. Constr Build Mater 2003;17(6–7):447–62.
[10] Zhang HW, Smith ST. Influence of FRP anchor fan configuration and dowel angle on anchoring FRP plates. Compos B Eng 2012;43(8):3516–27.
[11] Zhang HW, Smith ST. FRP-to-concrete joint assemblages anchored with multiple FRP anchors. Compos Struct 2012;94(2):403–14.
[12] Zhang HW, Smith ST, Kim SJ. Optimisation of carbon and glass FRP anchor design. Constr Build Mater 2012;32:1–12. Special Issue on Strengthening and Retrofitting of Concrete Structures with Fiber Reinforced Polymer Material.
[13] Zhang HW. Influence of FRP anchors on FRP-to-concrete bonded interfaces [Doctor of Philosophy Dissertation]. Hong Kong, China: University of Hong Kong; 2013.
[14] Chen JF, Teng JG. Anchorage strength models for FRP and steel plates bonded to concrete. J Struct Eng ASCE 2001;127(7):784–91.
[15] ACI 440.3R-04. Guide test methods for Fiber-reinforced Polymer (FRPs) for reinforcing or strengthening concrete structures. Farmington Hills, MI, USA: American Concrete Institute (ACI); 2004.
[16] BS EN ISO 527. Plastics-determination of tensile properties. UK: British Standards; 1996.
[17] BS 1881-116. Testing concrete. Method for determination of compressive strength of concrete cubes. UK: British Standards; 1983.
[18] BS 1881-117. Testing concrete. Method for determination of tensile splitting strength. UK: British Standards; 1983.
[19] BS 1881-118. Testing concrete. Method for determination of flexural strength. UK: British Standards; 1983.
[20] BS 1881-121. Testing concrete. Method for determination of static modulus of elasticity in compression. UK: British Standards; 1983.
[21] Kim SJ. Strengthening of reinforced concrete slabs with penetrations using unanchored and anchored Fibre-Reinforced Polymer (FRP) composites [Doctor of Philosophy Dissertation]. Sydney, Australia: University of Technology Sydney; 2009.
[22] Haskett M, Oehlers DJ, Ali MSM. Local and global bond characteristics of steel reinforcing bars. Eng Struct 2008;30(2):376–83.
[23] Zhang HW, Smith ST, Gravina RJ. Analysis of FRP-to-concrete interfaces using a displacement driven partial interaction model. Int J Mech Sci 2016;17:210–7.
[24] Zhang HW, Smith ST, Derivation of load-slip model for FRP anchors, 2013. In: Al-Mahaidi R, Smith ST, Bai Y, Zhao XL, editors. Proceedings (USB), Fourth Asia-Pacific Conference on FRP in Structures, APFIS 2013, Melbourne, Australia, 11–13 December 2013.